Cement and Concrete Research 197 (2025) 107952

Contents lists available at ScienceDirect

Cement and Concrete Research

journal homepage: www.elsevier.com/locate/cemconres

Retention of niobium(V) by calcite and carbonated cement paste: quantitative description and impact of isosaccharinic acid and chloride

Nils Huber [a,*], R.E. Guidone [a], X. Gaona [a,*], K. Garbev [b], M. López-García [c], L. Alcubierre [c], F. Bocchese [d], S. Brassinnes [d], M. Altmaier [a], H. Geckeis [a]

[a] Institute for Nuclear Waste Disposal, Karlsruhe Institute of Technology, Karlsruhe, Germany
[b] Institute for Technical Chemistry, Karlsruhe Institute of Technology, Karlsruhe, Germany
[c] Amphos 21, Barcelona, Spain
[d] ONDRAF/NIRAS, Belgian Agency for Radioactive Waste and Enriched Fissile Materials, Brussels, Belgium

ARTICLE INFO

Keywords:
Niobium(V)
Sorption
Calcite
Carbonated cement paste
Isosaccharinic acid (ISA)

ABSTRACT

Sorption experiments with niobium(V) in calcite and carbonated cement were conducted simulating cement degradation stage IV. ^{93}Nb and ^{95}Nb ($t_{1/2}$ = 35.0 days) were used as probes of ^{94}Nb ($t_{1/2} = 2{\cdot}10^4$ years), expected in nuclear waste. In calcite systems, an initial uptake ($R_d \approx 10^3$ L·kg^{-1} at t = 3 days) was followed by a steady increase of distribution ratios with time ($R_d > 2{\cdot}10^4$ L·kg^{-1} at t = 89 days). This was explained as fast adsorption, followed by slow incorporation into the calcite structure. The stronger uptake observed for carbonated cement is attributed to the presence of amorphous phases with larger surface area. The formation of complexes with isosaccharinic acid (ISA) slightly decreases Nb(V) sorption, whereas chloride has a minor effect on the uptake of Nb(V) up to 2.0 M NaCl. This work provides an improved quantitative description and mechanistic understanding of ^{94}Nb retention in repositories for nuclear waste.

1. Introduction

Niobium (Nb) is a rare element in the earth's crust (approximately 20 ppm), which occurs naturally as only one stable isotope (^{93}Nb) and is mainly found in the pentavalent oxidation state, *i.e.*, Nb(V) [1–3]. Niobium is used in structural components of nuclear power reactors such as Ni-based alloys and stainless steel. During reactor operation, the long-lived β-emitter isotope ^{94}Nb ($t_{1/2} = 2.04{\cdot}10^4$ a) is produced by neutron activation of ^{93}Nb, and it is accordingly present in certain waste streams resulting from the dismantling of such facilities. In the context of repositories for the disposal of low and intermediate level waste (L/ILW), ^{94}Nb was identified as relevant contributor to the effective dose potentially released to the biosphere, mostly due to the lack of relevant data and the conservative assumption of a weak retention [4].

Cementitious materials are widely used in repository systems for radioactive waste as structural components, encapsulants, and as immobilization/stabilization agents, particularly (but not exclusively) in repositories for L/ILW [5,6]. Besides their structural properties, cementitious materials exhibit a strong sorption capacity for various radionuclides, especially for metal cations. Depending on the country and repository concept, the disposal of L/ILW can be conceived in underground, near-surface or surface facilities, which influence the boundary conditions that the waste and engineered barriers will face within the regulatory lifetime of the repository.

The interaction of cementitious materials with intruding water leads to the dissolution and transformation of different cement phases, with the subsequent degradation of the cement and the induction of a pore water composition buffered in the alkaline to hyperalkaline pH range ($10 \leq pH \leq 13.5$) with moderate Ca concentrations. The degradation of Hydrated Cement Paste (HCP) is generally divided in four main stages. In degradation stage I, pore water composition is dominated by the dissolution of alkali metal (K and Na) oxides / hydroxides resulting in high pH values ($12.5 < pH < 13.5$). After the alkali ions have been leached out, the dissolution of portlandite ($Ca(OH)_2$) buffers the pore water in stage II at pH ≈ 12.5 and [Ca] ≈ 20 mM. Degradation stage III involves the incongruent dissolution of the calcium silicate hydrate (C-S-H) phases, during which the Ca/Si ratio in such phases decreases together with an overall decrease in pH of the pore water from 12.5 to ~10. In stage IV, C-S-H phases and other hydrated components are dissolved, and the pore water composition with pH < 10 is governed by

* Corresponding authors.
E-mail addresses: nils.huber@kit.edu (N. Huber), xavier.gaona@kit.edu (X. Gaona).

https://doi.org/10.1016/j.cemconres.2025.107952
Received 4 February 2025; Received in revised form 20 May 2025; Accepted 27 May 2025
Available online 6 June 2025

the equilibrium with the remaining aggregate minerals, *i.e.*, mostly calcite ($CaCO_3$) [5]. In the case of near-surface repositories, carbonation of cement has been also identified as one of the relevant chemical reactions, which mainly results in the formation of calcite, but also in smaller fractions of SiO_2(am), $Al(OH)_3$(am) and gypsum ($CaSO_4{\cdot}2H_2O$) [7,8]. Note that the four degradation stages defined above can be altered in blended cements with, *e.g.*, slag, silica fume or nanosilica, which can reduce the content of alkalis and overall inventory of portlandite in the hydrated cement [9,10].

In repositories for L/ILW, cellulose is often as part of the emplaced waste. Under the hyperalkaline conditions of the Ca-rich pore waters defined by cementitious systems, cellulose degrades and isosaccharinic acid (ISA, $C_6H_{12}O_6$) has been identified as one of its main degradation products. ISA forms stable complexes with a large number of metal ions, including actinides (in +III to +VI oxidation states) [11–13], lanthanides [11] and transition metals (*e.g.*, Ni, Zr, Fe, among others) [14–16], which may significantly affect sorption behaviour. Due to its several functional groups (1 -COOH, 4 -OH), ISA is able to outcompete hydrolysis and thus form stable complexes with strongly hydrolyzing metal ions, also in hyperalkaline pH conditions.

High concentrations of stable chloride (up to ≈ 4–5 M) have been described for specific waste streams containing evaporator concentrates from nuclear power plants operation [17]. Such high chloride concentrations may induce changes in the aqueous speciation of radionuclides, alter the composition and surface properties of the engineered barriers (*e.g.*, cement) and thus impact the retention properties of these radionuclides.

Several studies have investigated the uptake of Nb(V) by cementitious materials, including Portland cement (CEM I), blast furnace cement (CEM III/C) and C-S-H phases of different Ca/Si ratios [18,19]. With some exceptions as discussed in Jo et al. [20], most of these studies report a strong uptake ($R_d \approx 10^4$–10^6 $L{\cdot}kg^{-1}$), in line with the sorption behaviour of other strongly hydrolyzing metal ions, *e.g.*, Ln(III), M(IV) or An(IV/V/VI). On the other hand, no experimental studies are available to date targeting the uptake of Nb(V) by calcite, impacting predictions on the retention of this radionuclide in the degradation stage IV of cement. Based on systematic trends described for other radionuclides, Ochs and co-workers estimated upper and lower limits for distribution ratios of Nb(V) on calcite as $R_d \approx 5{\cdot}10^3$ $L{\cdot}kg^{-1}$ and $5{\cdot}10^1$ $L{\cdot}kg^{-1}$, respectively [5]. The recent work by Çevirim-Papaioannou, Jo and co-workers confirmed that ISA decreases the uptake of Nb(V) by CEM I and CEM III/C at pH ≈ 13.3–13.5 due to the formation of stable Nb(V)–ISA complexes, possibly involving the participation of Ca [18,20]. No studies on the complexation of Nb(V) with ISA are available so far in the pH conditions defined by calcite (pH ≈ 8.3), as expected in the degradation stage IV of cement.

In this context, this work aims at quantitatively evaluating the retention of Nb(V) under conditions relevant for the degradation stage IV of cement. The study targets the sorption of Nb(V) on commercial calcite and carbonated cement paste, including sorption kinetics, sorption isotherms and determination of distribution ratios (R_d values). The effect of ISA and chloride is also accounted for in a series of sorption experiments with the ternary (solid phase / Nb(V) / ISA and solid phase / Nb(V) / Cl^-) and quaternary (solid phase / Nb(V) / ISA / Cl^-) systems. The results are also discussed in terms of mechanisms driving the uptake of Nb(V), which include adsorption, incorporation and isotopic exchange reactions. Complementary experiments describing the solid phase formation and solubility behaviour of Nb(V) in calcite- and carbonated cement-equilibrated waters are reported elsewhere [21].

2. Experimental

2.1. Chemicals and analytical methods

All solutions were prepared under air with Milli-Q water (Millipore Milli-Q Advantage A10 (18.2 MΩ·cm at 25 °C, 4 ppb TOC with Millipore Millipak® 40 0.22 μm). Radioactive samples were prepared and stored in a glovebox under air. NaOH Titrisol, HCl Titrisol, calcite ($CaCO_3$, 99.0 %) were purchased from Merck. Niobium(V) chloride (99 %) was obtained from Sigma-Aldrich. A 0.25 mL active ^{95}Zr source ($t_{1/2}$ = 64.0 days) in 0.5 M oxalate solution was purchased from Eckert & Ziegler Nuclitec GmbH with an initial activity of 2.68 MBq of ^{95}Zr. Because of the age of the ^{95}Zr source, a significant in-growth of ^{95}Nb ($t_{1/2}$ = 35.0 days) had taken place, resulting in 3.62 MBq of ^{95}Nb. These activities in the mother stock correspond to $[^{95}Zr]_{tot} = 1.42{\cdot}10^{-7}$ M and $[^{95}Nb]_{tot} = 1.05{\cdot}10^{-7}$ M. The concentrations of the inactive isotopes in the stock solution were quantified as $[Zr]_{tot} = (8.8 \pm 0.2){\cdot}10^{-2}$ M and $[Nb]_{tot} \leq 1.7{\cdot}10^{-6}$ M. The inactive Nb(V) stock solution was prepared by dissolving $NbCl_5$ in 0.2 M NaOH.

Isosaccharinic acid-1,4-lactone was purchased at Biosynth and dissolved in 4 M NaOH (Tritisol, Merck). After pH adjustment with HCl (Titrisol, Merck), the ISA stock was prepared with a concentration of 1.73 M ISA at pH ≈ 12. The resulting ISA solution was characterized by means of ^1H and ^{13}C Nuclear Magnetic Resonance (NMR) spectroscopy (Bruker Avance III 400 spectrometer, operating at 400.18 MHz for ^1H and 100.63 MHz for ^{13}C), Inductively Coupled Plasma Optical Emission Spectroscopy (ICP-OES, Na and Ca), non-purgeable organic carbon (NPOC) and total inorganic carbon (TIC), as well as inductively coupled plasma mass spectrometry (ICP-MS) for the quantification of the total metal content. The ^1H NMR spectra (see Fig. SI-1 in the Supporting Information) confirmed the complete transformation of the lactone in the open chain form, as well as the purity of the final ISA product.

The pH values were measured using a ROSS Orion combination pH electrode with 3.0 M KCl as filling solution. Electrode calibration was performed with standard buffers (7–12, Merck). For the quantification of the active ^{95}Nb, gamma spectrometry measurements were performed using a high purity germanium detector (61 mm × 46 mm, Mirion) with an energy resolution of 1.8 keV at 1.33 MeV and 0.875 keV at 122 keV, and a built-in autosampler (IMPROMAT, Belgium). The detector calibration range was 45–1800 keV using an Eckert and Ziegler multi-element standard as calibration solution. The sample geometry was defined by 10 mL PP flasks (Kautex, a Textron Company) with total sample volume of 10 mL. The ^{95}Nb isotope ($t_{½}$ = 35.0 days) was quantified following the 765 keV gamma line. The measurement time was set to 2 h. The detection limit for this isotope and gamma lines was 0.26–0.38 $Bq{\bullet}mL^{-1}$ for a measuring time of 2 h. Considering the dilution steps, this corresponds to a detection limit of $[^{95}Nb] \approx 1.5{\cdot}10^{-12}$ M.

2.2. Preparation and characterization of calcite, degraded cement paste and corresponding equilibrated waters

The commercial calcite considered in this work was used as purchased without further pre-treatment, besides a sieving step to <63 μm. The resulting material was characterized by X-ray diffraction (XRD), scanning electron microscopy with energy dispersive X-ray spectroscopy (SEM-EDX) and Brunauer-Emmett-Teller (N_2-BET) surface area analysis. XRD measurement was conducted with a Bruker AXS D8 Advance X-Ray Powder Diffractometer (LYNXEYE XE-T detector) at 2θ = 5–60° with incremental steps of 0.0012° and a measurement time of 0.25 s per step.

For BET measurements, calcite and carbonated cement paste were dried at 60 °C under oil pump vacuum for approximately 12 h. Multipoint BET measurements were performed varying nitrogen p/p_0 from 0.05 to 0.30 ($0.05 < p/p_0 < 0.30$) using 3P instruments micro 200B BET surface area and porosity analyzer.

SEM images were taken with secondary electrons by an Everhart-Thornley SE detector (accelerating voltage 2 kV, store resolution 4096 × 3072 pixel and various magnifications from 200× to 30,000×) for morphology. For the measurement, the calcite sample was prepared by dusting powder onto double-sided adhesive C-tab SEM and fixed onto an 8 mm Al rod.

Calcite-equilibrated water was prepared by contacting commercial $CaCO_3$ with Mili-Q water under air for at least one week at a solid to

liquid ratio (S/L) of 1 $g{\cdot}L^{-1}$. The equilibrated water composition was characterized by pH measurements and the determination of Ca concentration (ICP-OES) and total inorganic carbon concentration (TIC). These results were compared with the target values calculated assuming equilibrium with atmospheric $CO_2(g)$ and using the thermodynamic data selection in the ThermoChimie database [22], *i.e.*, pH = 8.3, [Ca] = $5.8{\cdot}10^{-4}$ M and $[C]_{tot} = 1.21{\cdot}10^{-3}$ M (see Section 3.1). Before use, the calcite-equilibrated water was separated from the solid phase by centrifugation (10 min, 6000 rpm). The content of ^{nat}Nb in calcite was quantified in triplicate by dissolving 240 mg of the material in 0.1 M HNO_3, followed by ICP-MS measurements.

The carbonated and leached cement paste was prepared as follows. First, hydrated cement paste (HCP) was prepared using CEM I (provided by ONDRAF-NIRAS) with a water to cement ratio of 0.46 ($L{\cdot}g^{-1}$) and a curing time of 28 days. After curing, the hydrated cement paste was crushed and grinded to obtain a powder with a particle size lower than 200 μm. This powder was mixed with water at a solid to liquid ratio (S/L) of 1000 $g{\cdot}L^{-1}$, and flushed in a closed reactor with a gas mixture CO_2 / N_2 of 30/70 % for 85 h under continuous magnetic stirring. Regular additions of 10 mL of water were done every 24 h. The resulting material was dried at 50 °C for two days, and characterized by means of confocal Raman spectroscopy, XRD, IR-ATR and BET measurements.

Powder X-ray diffraction for determination of the phase composition of the carbonated cement paste was performed with Empyrean diffractometer (Malvern-Panalytical) operated with a Cu tube and power of 1.6 kW. The measurements were carried out using backloading sample holders in reflection geometry in the range 5–100° 2theta with a step size of 0.0131°2theta. The measurement time was 100 s/step. Fixed slit of size 1/8° and soller slits (0.04Rad) on both optical paths were used. Kβ radiation was eliminated with Bragg-BrentanoHD device. A multistrip PIXcel3D detector with a simultaneous acquisition range of 3.348° 2theta was employed for detection. The phase identification was carried out with HighScore-plus v.5 software (Malvern-Panalytical). Rietveld refinement was performed with TOPAS 7 (Bruker-AXS) using fundamental parameters approach. The full list of the structure data for the phases used as a starting model and corresponding references is shown in the Supporting Information file (Table SI-1). The amorphous content was calculated with external standard (Si) using the corresponding K-factor. The size of the coherent scattering domains was evaluated by the double Voigt approach.

Infrared spectroscopy with Attenuated Total Reflection (IR-*ATR)* was used to characterize the carbonated cement paste on a SPECAC Golden Gate ATR device with a diamond crystal. Spectra were obtained with a TENSOR II FT spectrometer (Bruker Optics, Ettlingen, Germany) in the range 600-4000 cm^{-1} with 64 scans and spectral resolution of 2 cm^{-1}.

The carbonated cement paste was contacted with deionized water for 14 days, and the solution characterized with the measurement of pH, concentration of metal ions and anionic species, resulting in [Ca] = $(4.9 \pm 0.7){\cdot}10^{-3}$ M, [Na] = $(5.4 \pm 0.8){\cdot}10^{-4}$ M, [K] = $(2.1 \pm 0.3){\cdot}10^{-3}$ M, [Mg] = $(4.1 \pm 1.0){\cdot}10^{-4}$ M, [Si] = $(6.5 \pm 1.0){\cdot}10^{-4}$ M, [Al] = $(2.6 \pm 0.3){\cdot}10^{-4}$ M, $[Cl^-] = (8.9 \pm 0.1){\cdot}10^{-3}$ M, $[SO_4^{2-}] = (2.4 \pm 0.3){\cdot}10^{-3}$ M, TIC = $(2.7 \pm 0.6){\cdot}10^{-4}$ M. Based on this water composition, artificial carbonated cement water was prepared by dissolving calcium chloride, sodium bicarbonate and amorphous silica in Milli-Q water targeting $[Ca]_{tot} = 3.0{\cdot}10^{-3}$ M, $[C]_{tot} = 2.03{\cdot}10^{-4}$ M and $[Si]_{tot} = 8.35{\cdot}10^{-5}$ M, with pH ≈ 8.4–8.5. The concentration of Ca in the artificial carbonated cement water was slightly decreased to avoid oversaturation conditions and the possible precipitation of calcite.

The ^{nat}Nb content in the carbonate cement paste was quantified by means of alkaline fusion. A precise weight of carbonated cement paste (200 mg) was mixed with potassium hydroxide pellets in a platinum/gold crucible, and the mixture was melted at 390 °C for 15 min. Milli-Q water was added while stirring to wash out all of the dissolved mixture. The solution was acidified with 32 % HCl and then diluted with water for ICP-MS measurements. In the calcite system, 0.241 g of the solid material were dissolved in 60 mL of a 0.1 M HCl solution, and the Nb concentration quantified with ICP-MS.

The concentrations of Nb leached by calcite and carbonated cement paste after 2 days of equilibration time with the corresponding pore waters were measured by Inductively Coupled Plasma Mass Spectrometry (ICP-MS) after ultrafiltration (10 kDa, 2–3 nm cut-off Nanostep®, Pall Life Sciences).

Confocal Raman spectroscopic single spot measurements and area mappings of the carbonated cement paste were performed on a WITec alpha300 R instrument equipped with UHTS300 spectrometer (300 mm focal length) and Zeiss microscope. 488 nm and 532 nm lasers operated by adjustable TruePower modules in the range between 10 and 40 mW (measured on the sample) was used as an excitation source. Single spot measurements were performed with a 100× objective (NA = 0.9) using 600 and 1800 g/mm gratings. The corresponding spectral resolution was better than 3 cm^{-1} and 1 cm^{-1}, respectively. The detection of the Raman scattering was carried out with a back illuminated CCD Camera. Typical acquisition times were between 5 and 10 s. with 5–10 scans. The data processing was performed with the Project 6.1 + software and included cosmic ray removal and background subtraction with a shape algorithm. WITec TrueMatch program with integrated RRUFF mineral database and own database was used for the purposes of phase identification. Between 20 and 45 spectra per sample were taken at different sample positions. Averaged spectra were used for band assignment and to emphasize the differences between them. An area mapping 200 × 140 μm was performed on a pressed powder sample with a step size of 1 μm. Thus, the hyperspectral stack consisted of 28,000 single spectra collected with automatic focusing on the sample surface. The Raman image of the lateral distribution of the mineral constituents was delivered by integration in the corresponding frequency ranges typical for given phase.

2.3. Sorption experiments: Binary, ternary and quaternary systems

All sorption experiments were performed in 15 mL vials (Sarsted®) with a total volume of 10 mL. All samples were prepared, stored and handled in a glove box with air atmosphere. Calcite and carbonated cement paste systems were investigated in six and five independent series, respectively, as described in Table 1. Sorption samples were prepared by spiking a combination of ^{93}Nb and ^{95}Nb to the calcite or carbonated cement paste suspensions, which were previously equilibrated with the corresponding solutions for 2 days. The pH was adjusted (using HCl and NaOH) to 8.2–8.4 and 8.3–8.5 in the calcite and carbonated cement paste systems, respectively. For the ternary systems involving chloride, the calcite or carbonated cement paste suspension was equilibrated for 3 days with the required amount of NaCl, before adding the combination of ^{93}Nb and ^{95}Nb. The ternary system including ISA was prepared adding ISA 3 days after the spiking of the combination of ^{93}Nb and ^{95}Nb. Quaternary experiments were performed adding chloride 3 days prior to the spiking of Nb, and adding ISA 3 days after the spiking of Nb. Most of the sorption samples were prepared in duplicates.

After a given contact time (see Table 1), two aliquots of the supernatant (*ca.* 4.2 mL each) of each sample were ultracentrifuged at 90,000 rpm and 20 °C for 1 h (Type 90 Ti rotor and OptimaTM XPN-90, Beckman Coulter) to separate suspended particles and colloids. To determine the concentration of ^{95}Nb in the aqueous phase, approximately 3.5 mL of supernatant was collected with a syringe, transferred to 10 mL LDPE vials and diluted in 2 % HNO_3 for gamma spectrometry. The uncertainty of the gamma measurements was ±5–10 %. The sorption of Nb(V) on the vessel walls was quantified for selected samples (calcite, carbonated cement paste) after the completion of the sorption experiments. The vials were emptied, washed with water three times and filled with 1 M HCl to leach the sorbed Nb(V). After 1 day, the niobium concentration was measured by gamma spectroscopy. In the absence of chloride, the Nb sorbed to the walls of the Starsted® vials was quantified as ≈ 11 % of the initial activity, which was taken into account in the calculation of the

Table 1
Experimental conditions considered in the sorption experiments with calcite and carbonated cement paste for the binary, ternary and quaternary systems.

Type of experiment	Sorbing material	$A(^{95}Nb)_0$ [kBq]	Contact time [days]	S/L [$g \cdot L^{-1}$]	$[Nb]_{tot}$ [M]	$[Cl^-]_{tot}$ [M]	$[ISA]_{tot}$ [M]	Number of samples*
Binary system: Nb(V) sorption kinetics	Calcite	0.05	3–85	1	$1 \cdot 10^{-9}$	$5.84 \cdot 10^{-4}$	–	6
Binary system: Nb(V) sorption isotherm	Calcite	0.05	3	1	$1 \cdot 10^{-11}$–$1 \cdot 10^{-6}$	$5.84 \cdot 10^{-4}$	–	11
Binary system: Impact of S/L on Nb(V) uptake	Calcite	0.1	3–10	5, 10	$1 \cdot 10^{-9}$	$5.84 \cdot 10^{-4}$	–	4
Ternary system: Impact of ISA on Nb(V) uptake	Calcite	0.05	3	1	$1 \cdot 10^{-9}$	$5.84 \cdot 10^{-4}$ –$1.3 \cdot 10^{-3}$	$1 \cdot 10^{-5}$–0.1	5
Ternary system: Impact of Cl^- on Nb(V) uptake	Calcite	0.05	3	1	$1 \cdot 10^{-9}$	$5.84 \cdot 10^{-4}$–2	–	7 (11)
Quaternary system: Impact of ISA + Cl^- on Nb(V) uptake	Calcite	0.05	3	1 5, 10	$1 \cdot 10^{-9}$ $1 \cdot 10^{-9}$	$5.84 \cdot 10^{-4}$–2 1–2	$1 \cdot 10^{-2}$	6 (11)
Binary system: Nb(V) sorption kinetics	Carbonated cement paste (CEM I)	1.7	3–54	1	$1 \cdot 10^{-9}$	$4.2 \cdot 10^{-9}$	–	5
Binary system: Nb(V) sorption isotherm	Carbonated cement paste (CEM I)	2	3	1	$1 \cdot 10^{-8}$–$1 \cdot 10^{-6}$	$4.2 \cdot 10^{-9}$	–	9
Ternary system: Impact of ISA on Nb(V) uptake	Carbonated cement paste (CEM I)	2	3	1	$1 \cdot 10^{-9}$	$3.9 \cdot 10^{-4}$–$3.2 \cdot 10^{-3}$	$1 \cdot 10^{-5}$ – $1 \cdot 10^{-2}$	5 (9)
Ternary system: Impact of Cl^- on Nb(V) uptake	Carbonated cement paste (CEM I)	2	3	1	$1 \cdot 10^{-9}$	$5.0 \cdot 10^{-2}$ – 2	–	4 (8)
Quaternary system: Impact of ISA + Cl^- on Nb(V) uptake	Carbonated cement paste (CEM I)	2	3	1	$1 \cdot 10^{-9}$	$2.3 \cdot 10^{-2}$ – 2	$1 \cdot 10^{-2}$	6

* Values in parentheses correspond to total number of samples including replicates.

Nb concentration and quantification of the distribution ratios (R_d in $L \cdot kg^{-1}$) by subtracting from the initial activity before calculation. This effect was negligible in samples containing NaCl concentrations ≥1 M. The presence of ISA did not result in significant deviations with respect to ISA-free systems.

The uptake of Nb(V) by calcite and carbonated cement paste in the absence and presence of ISA and chloride was evaluated in terms of sorption isotherms (log ($[Nb]_{solid}$) *vs.* log ($[Nb]_{aq}$)) and R_d values. R_d values were determined as the ratio of the niobium concentration in the solid (c_{solid} in $mol \cdot kg^{-1}$) and in the aqueous phase (c_{aq}, in M):

$$R_d = \frac{C_{solid}}{C_{aq}} = \frac{(A_{inital} - A_{aq})}{A_{aq}} \cdot \frac{V}{m} \quad (1)$$

where A_{inital} is the initial niobium activity in $[Bq \cdot mL^{-1}]$, A_{aq} is the activity in the aqueous phase after phase separation in $[Bq \cdot mL^{-1}]$, V is the volume of the sample in [L], and m is the mass of calcite used in the experiment in [kg]. For the uncertainties in the R_d values, the error of the gamma measurement was considered and calculated as two times the standard deviation of independent measurements. Uncertainty in the gamma measurements was in most cases <5 %, and has been thus disregarded in the calculation of the overall R_d uncertainty.

3. Results and discussion

3.1. Characterization of calcite, carbonated cement paste and equilibrated waters

XRD analysis shows that the calcite is highly crystalline (Fig. SI-2a). SEM observations show a heterogeneous particle distribution with size <60 μm (see Fig. SI-2b).

The specific surface area of the calcite is ≈ 0.7 $m^2 \cdot g^{-1}$, as determined by BET measurements. The size and surface area of the commercial calcite used in this work are in line with those reported by Heberling and co-workers for a coarse commercial calcite (supplied also by Merck) [23].

Carbonated cement paste was characterized by quantitative X-ray diffraction (QXRD) with external standard in order to account for amorphous constituents. Fig. 1 shows the Rietveld plot and the constituents in this sample. Additional information about the results of the Rietveld refinement including R values, estimated standard deviations, *etc.* can be found in Table SI-2 in the Supporting Information.

Rietveld analysis of the carbonated cement paste confirms calcite as main constituent. Minor phases are some unreacted C_2S (larnite), brownmillerite as well as impurities as quartz. The presence of $CaSO_4$ as gypsum and anhydrite (and possibly basanite) points to accelerated carbonation of the AFm and AFt phases and subsequent formation of sulphates, hydrogarnets (katoite) and LDH phases, as partly described by Kalkreuth and co-workers [24]. As a result of the carbonation of the C-S-H phase, SiO_2 gel along with carbonate is formed. Therefore, the biggest part of the amorphous content found in the sample (26.4 wt%) could be assigned to this gel. Presence of amorphous carbonate could not be excluded although the probability for this seems to be low given the carbonation conditions. The size of the coherent scattering domains of calcite obtained by the double Voigt approach is 67 nm, *i.e.*, a significantly smaller crystallite size compared to the commercial calcite (average crystallite size ~200 nm obtained using Scherrer's equation) used in this work. The specific surface area of the carbonated cement was quantified as ≈ 60 $m^2 \cdot g^{-1}$, *i.e.*, ~ 100 times greater than the surface area determined for the calcite material used in this work.

Fig. 2 shows the IR-ATR spectrum of the carbonated cement paste together with spectra of some selected constituents. It can be seen that along the strongest bands of calcite (712 cm^{-1}, 872 cm^{-1} and 1406 cm^{-1} assigned to ν_4, ν_2 and ν_3 vibrations of CO_3^{2-}, respectively), a broad absorption in the range 950–1250 cm^{-1} is present. It is assigned to Si—O vibrations typical for C-S-H or/and SiO_2 gel. Small contributions from quartz and ν_3-SO_4 are expected to the middle and high frequency part of

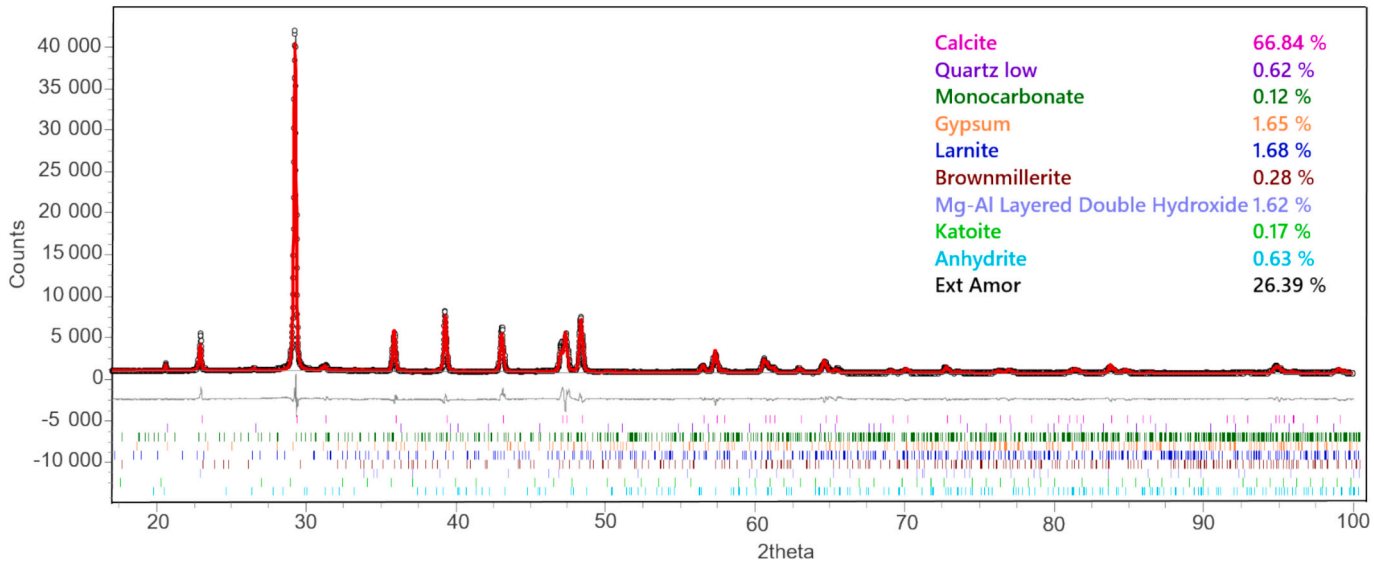

Fig. 1. Rietveld plot and quantitative analysis of the carbonated cement paste (CEM I).

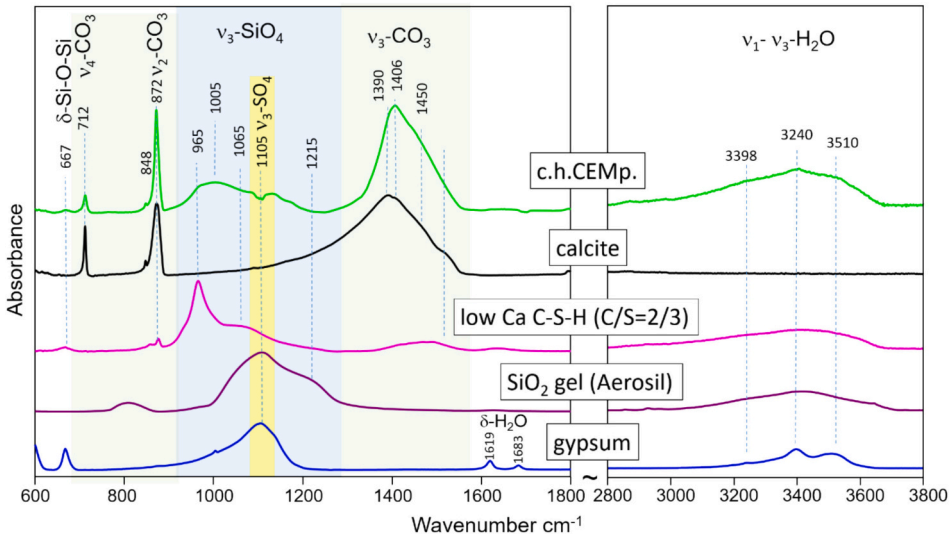

Fig. 2. IR-ATR of carbonated cement paste (c.h.CEMp.) compared to single spectra of calcite, low C/S ratio C-S-H, SiO_2 gel, and gypsum.

the range. Depending on the C/S ratio, the C-S-H phase contributes in the range 940–965 cm^{-1}. In this particular case, there is an increased absorption at 965 cm^{-1} which shows a remarkable coincidence with the main Si—O band of synthetic C-S-H phase prepared with C/S = 2/3 (Fig. 2, middle spectrum). Comparison of the observed frequency for the SiO_2 gel (1070 cm^{-1}) of fully carbonated hydrated cements and the IR-ATR spectra of this study (1005 cm^{-1}) implies that probably there is indeed some C-S-H phase with very low C/S ratio is still present in the sample [24,25]. On the other hand, the frequency of the Si—O vibration in the spectrum of pure SiO_2 (unfortunately overlapping with ν_3-SO_4 of gypsum) lies at higher frequency (1105 cm^{-1}). The discrepancies between the main frequencies of the gels product of carbonation of cementitious C-S-H phases on one hand, and these of pure SiO_2 gels on the other, imply that additional presence of both, Al and remnants of C-S-H phases influences the band positions in the IR-ATR spectra. Their quantity strongly depends on the degree of carbonation of the cement paste. For the reason of simplicity, we will further refer to this gel as "SiO_2 gel", but keeping in mind the differences compared to pure SiO_2 amorphous compounds. The presence of C-S-H phase in the carbonated cement is further confirmed by the enhanced signal in the region 3000–3800 $cm^{-1}$of the IR-ATR spectra, with clearly superimposed bands typical for gypsum at 3240 cm^{-1} and 3510 cm^{-1} (see Fig. 2).

Raman map of the carbonated cement paste confirms the findings of XRD and IR-ATR spectroscopy, providing additional information about the presence of a minor fraction of modified calcite (close to ankerite) in some areas of the sample. Fig. 3a shows a Raman image (200 × 140 μm) of the carbonated cement paste taken on a powder sample pressed onto a glass slide. The main constituent is calcite (red) along with larger unreacted particles of dicalcium silicate (C_2S, blue) and quartz (magenta). Different sulfates, mostly gypsum and anhydrite are spread throughout the sample as single particles or aggregates (both shown in green and referenced to as gypsum). In addition to pure calcite, a modified $CaCO_3$ with the same symmetry is clearly seen (light blue) differing from the former by (i) a shift to lower frequency of all bands, largest for the lattice vibration bands (LV1, 8 cm^{-1} and LV2, 11 cm^{-1}), and (ii) substantially broader bands in terms of full width at half maximum (FWHM) (Fig. 3c and d). The LV bands show the largest differences, implying differences in the cationic composition. The latter may induce defect structure thus influencing both the crystal size and surface area. Assuming some incorporation of impurities in the calcite

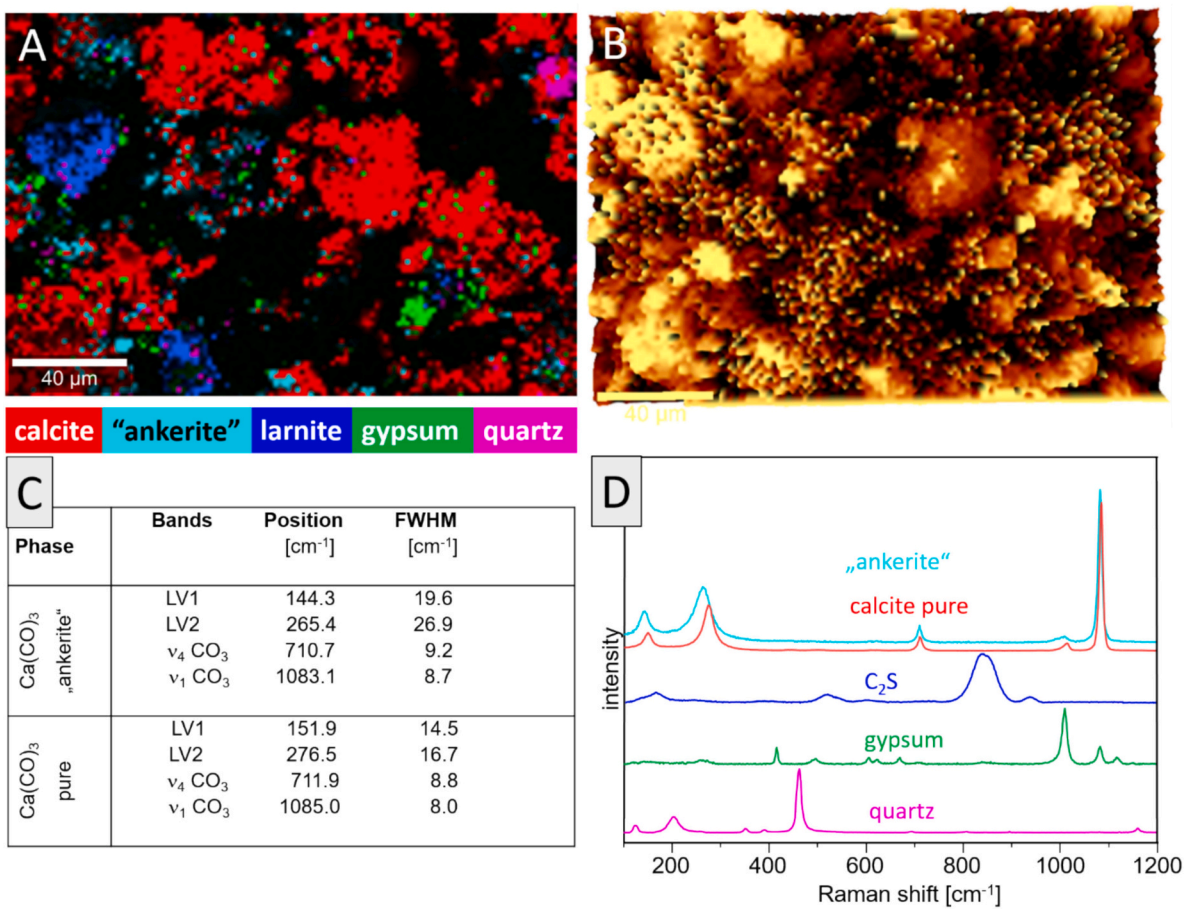

Phase	Bands	Position [cm^{-1}]	FWHM [cm^{-1}]
$Ca(CO)_3$ „ankerite"	LV1	144.3	19.6
	LV2	265.4	26.9
	ν_4 CO_3	710.7	9.2
	ν_1 CO_3	1083.1	8.7
$Ca(CO)_3$ pure	LV1	151.9	14.5
	LV2	276.5	16.7
	ν_4 CO_3	711.9	8.8
	ν_1 CO_3	1085.0	8.0

Fig. 3. (a) Raman image of the distribution of the main phases in the carbonated cement paste; (b) Corresponding topographic image of the same area; (c) Table of the band positions and FWHM of two different calcite species: calcite pure and "ankerite"; (d) Spectra of the main constituents in the Raman image.

structure during carbonation in presence of Mg and Fe "leftovers" from the hydrated products, we refer to this phase as a "ankerite", based on its complex composition, $Ca(Fe,Mg,Mn)(CO_3)_2$.

The characterization of the calcite- and carbonated cement paste-equilibrated waters is summarized in Table 2. For both materials, measured values confirm equilibrium (or steady-state) conditions already at $t = 2$ days. The quantification of Nb(V) in the equilibrated waters resulted in both cases below the detection limit of ICP-MS and considering the dilution steps used (Table 2). The concentration of natural Nb present in both solid materials was quantified as $[^{nat}Nb]_{solid} = 3.2{\cdot}10^{-5}$ mol·kg^{-1} (3 ppm; carbonated cement paste) and $[^{nat}Nb]_{solid} < 2.1{\cdot}10^{-9}$ mol·kg^{-1} ($< 2{\cdot}10^{-4}$ ppm; calcite, corresponding to the detection limit of the ICP-MS and considering the dilution steps used after alkaline fusion). The concentration of ^{nat}Nb quantified in carbonated cement is in line with the content of ^{nat}Nb previously reported for different cement pastes, *i.e.*, CEM I, CEM III-B and CEM III-C, ranging from 3.1 to 7.6 ppm [5,20,26].

3.2. Uptake of Nb(V) by calcite and carbonated cement paste in the absence of ISA

Fig. 4a shows the kinetics for the uptake of Nb(V) by calcite and carbonated cement paste, expressed in terms of distribution ratios (R_d) *vs.* time. A fast uptake is quantified for the uptake of Nb(V) by calcite at $t = 3$ days ($R_d \approx 10^3$ L·kg^{-1}, independently of the S/L ratio), followed by a steady increase in the uptake with time ($R_d > 2{\cdot}10^4$ L·kg^{-1} at $t = 89$ days). These observations are tentatively explained as a fast adsorption of Nb(V) on the calcite surface, followed by a slow incorporation driven by calcite recrystallization. A similar interpretation was given by Heberling and co-workers for the uptake of Np(V) by a commercial calcite material with a slightly higher surface area (1.3 m^2·g^{-1}) [27]. Note that the incorporation of several di- and trivalent cations (Cd^{2+}, Zn^{2+}, Co^{2+}, Cu^{2+}, Ni^{2+}, Eu^{3+}, Am^{3+}, Cm^{3+}, UO_2^{2+}, etc) into calcite has been extensively reported in the literature [28–31]. Although no laboratory studies are available on the incorporation of Nb in calcite, the presence of Nb in calcite and dolomite carbonatites might be considered as indication for such retention process [32].

Greater R_d values are determined for the uptake of Nb(V) by

Table 2
Composition of calcite- and carbonated cement paste-equilibrated waters.

Solid phase	pH	[Ca] [mol·L^{-1}]	C_{tot} [mol·L^{-1}]	[Si] [mol·L^{-1}]	[Nb] [mol·L^{-1}]
Calcite	8.2–8.4	$(5.8 \pm 0.1){\cdot}10^{-4}$	$(1.2 \pm 0.1){\cdot}10^{-3}$	n.m.[a]	$< 1.2{\cdot}10^{-11}$
Carbonated cement paste (CEM I)	8.3–8.5	$(3.0 \pm 0.1){\cdot}10^{-3}$	$(2.1 \pm 0.2){\cdot}10^{-4}$	$(5.5 \pm 0.3){\cdot}10^{-5}$	$\leq 1.3{\cdot}10^{-10}$

[a] Concentration not measured.

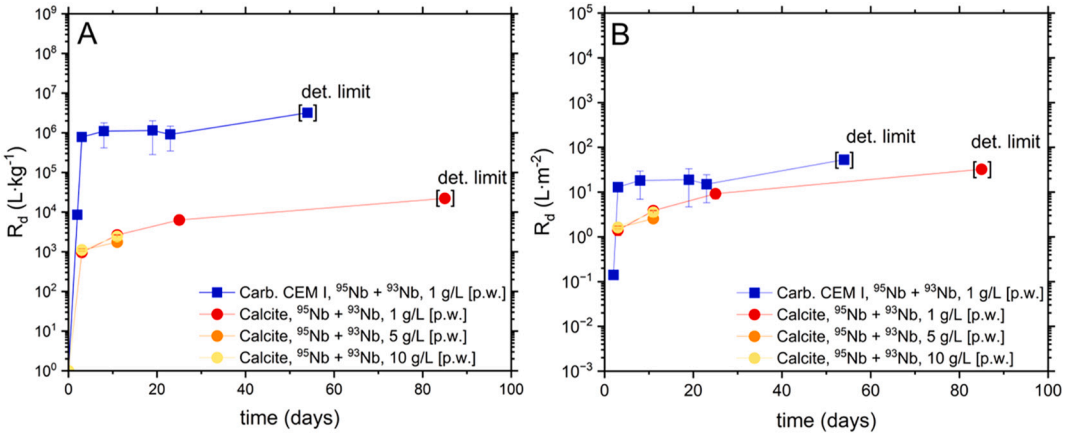

Fig. 4. Kinetics for the uptake of Nb(V) by calcite and carbonated cement. Initial Nb(V) concentration (as ^{93}Nb + ^{95}Nb) is $1.0{\cdot}10^{-9}$ M for all systems: (a) R_d values expressed in L·kg^{-1}; (b) R_d values normalized with respect to the specific surface area of the used materials expressed in L·m^{-2}.

carbonated cement paste, with R_d values of ~$8{\cdot}10^5$ L·kg^{-1}. This strong uptake is obtained after $t \geq 3$ days and is consistent up to $t = 23$ days. After 54 days the activity measured is below the limit of detection, resulting in slightly higher R_d values compared to the uptake at shorter contact times. The fast uptake observed for Nb(V) is consistent with recent studies on niobium uptake by hardened cement paste and C-S-H phases [18,20].

The large differences in the R_d values determined for both materials can be harmonized when normalizing the distribution coefficients by the specific surface area determined by BET for both materials, as shown in Fig. 4b. These results emphasize the need of an adequate knowledge of the surface properties (especially, but not exclusively, surface area) when interpreting sorption phenomena, particularly when different materials are compared.

Fig. 5 shows the sorption isotherms obtained in this work for the uptake of Nb(V) by calcite and carbonated cement paste. The figure includes also the sorption isotherm reported by Jo et al. [33] for the uptake of Nb(V) by calcium silicate hydrate (C-S-H) phases with a calcium-to-silicon ratio (C/S) of 1.4. The blue region in the figure marks the range of Nb(V) concentrations measured in the oversaturation solubility experiments after an equilibration time of 3 days, as reported in Huber et al. (2025). This supports that most of the experimental data points in the sorption isotherms are well below the solubility limit at pH ≈ 8.3. A linear sorption behaviour is confirmed for the uptake of Nb(V) by calcite over >4 orders of magnitude in aqueous niobium concentration. In the case of carbonated cement paste, the linearity range is limited at low concentrations due to the content of ^{93}Nb present in pristine cement (see Section 3.1). The linear trends observed in this work for calcite and degraded cement systems are in line with sorption data reported by Jo and co-workers for C-S-H phases, which show however a stronger sorption compared to the carbonated cement paste and (specially) to the calcite investigated in this work. Note however that this observation refers to absolute sorption values and does not account for differences in the surface area of the different materials. Although Jo and co-workers did not report the surface area of C-S-H phases used in their study, average values reported in the literature (≈ 150 m$^2{\cdot}$g^{-1} [34]) reflect a significantly higher surface area than the solid phases used in this study (calcite ≈ 0.7 m$^2{\cdot}$g^{-1} & carb. CEM I ≈ 60 m$^2{\cdot}$g^{-1}).

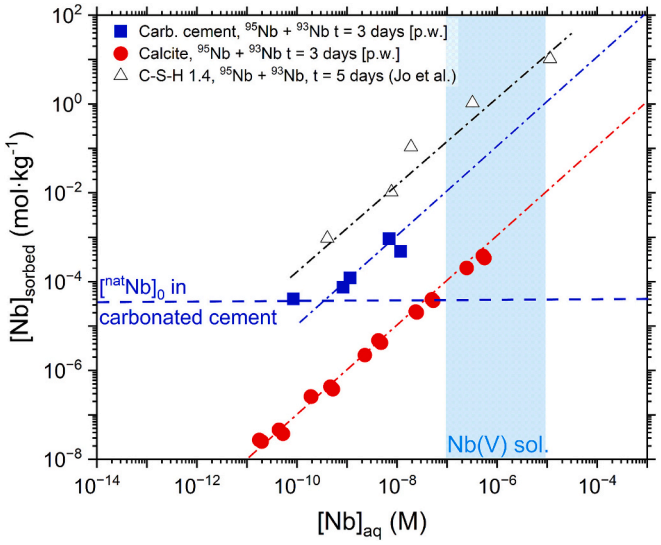

Fig. 5. Sorption isotherms for the uptake of Nb(V) by calcite (this work), carbonated cement paste (this work) and C-S-H 1.4 (Jo et al. [33]). All experiments conducted at S/L = 1 g·L^{-1}. Nb(V) added as combination of ^{93}Nb and ^{95}Nb. Blue region defines the range of Nb(V) concentrations determined after 3 days in the oversaturation solubility experiments at pH ≈ 8.3 and [Ca] ≈ $5.8{\cdot}10^{-4}$ M. Dashed horizontal line marks the concentration of ^{93}Nb in the carbonated cement (see Section 3.1). (For interpretation of the references to colour in this figure legend, the reader is referred to the web version of this article.)

Fig. 6 shows the comparison of the R_d values determined in this work for the uptake of Nb(V) by calcite ($t = 3$ and 89 days) and carbonated cement paste (t = 3 and 54 days), with distribution ratios reported in the literature for the uptake of Nb(V) by cement and C-S-H phases [26,33,35–37]. For R_d values expressed in [L·kg^{-1}], Fig. 6 confirms a much weaker uptake of Nb(V) by the calcite at short equilibration times, which is 2–3 orders of magnitude lower than those determined in this work for carbonated cement paste or reported in the literature for CEM I, CEM III or C-S-H phases. As discussed above, the evident increase in the R_d values determined for the calcite system at longer equilibration times can be potentially attributed to the incorporation of Nb into calcite. Experimental data determined in this work for calcite at short contact times are in agreement with estimated values provided by Ochs et al. (red square in Fig. 6) [5]. These authors indicated that "*There were no data for State IV, but lower sorption onto calcite would be expected. R_d values generally two orders of magnitude lower [than for State I-III] were chosen*". We thus provide the first experimental validation of this hypothesis, although acknowledging that at long contact times higher distribution ratios are to be expected for the calcite system.

Characterization methods discussed in Section 3.1 as well as thermodynamic calculations discussed in the literature [8] indicate that nano-particulate calcite and silica gel are the main components of the carbonated cement paste. The larger surface area offered by both materials as well as by remnants of C-S-H is expectedly responsible for the

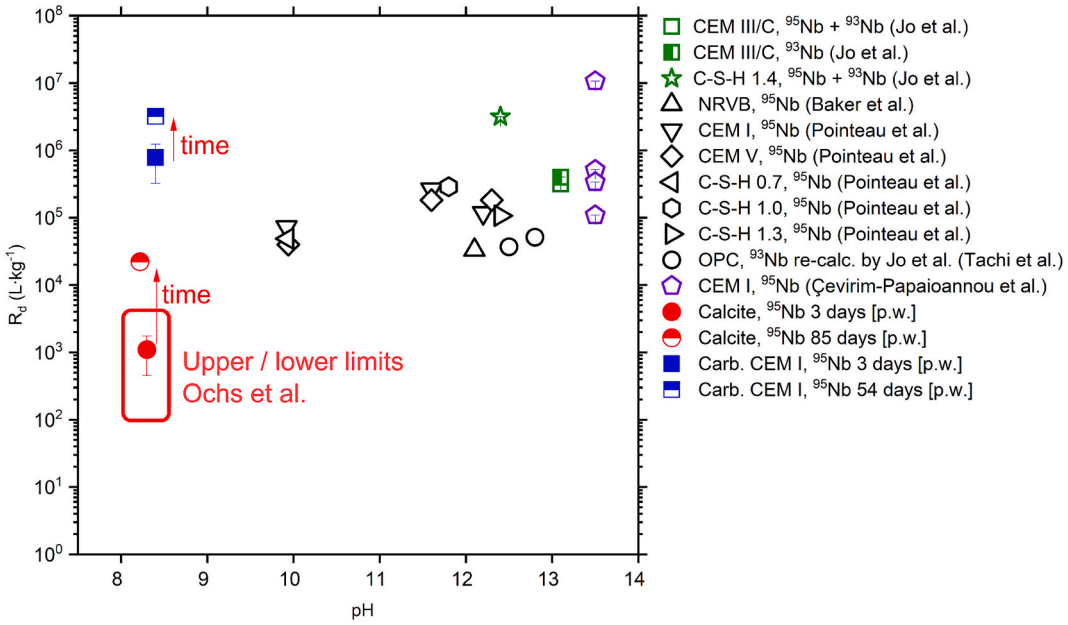

Fig. 6. Distribution coefficients determined in this work for the uptake of Nb(V) by calcite and carbonated cement, or reported in the literature for CEM III/C and C-S-H 1.4 [33], NRBV [35], CEM I, CEM V and C-S-H [36], OPC [37], or CEM I [18]. Red square in the figure defines the upper and lower R_d limits estimated in Ochs et al. [5]. (For interpretation of the references to colour in this figure legend, the reader is referred to the web version of this article.)

very strong uptake of Nb by carbonated cement paste. As discussed above, the normalization of the R_d values with respect to the surface area of the sorbing material offers a relevant perspective to interpret sorption phenomena and compare the sorption behaviour of different materials.

3.3. Uptake of Nb(V) by calcite and carbonated cement paste in the presence of ISA and chloride

Fig. 7 shows the distribution ratios for the uptake of Nb(V) by calcite and carbonated cement paste in the presence of increasing ISA concentrations. For comparison purposes, the figure includes also sorption data for the uptake of Nb(V) by cement paste CEM I in the presence of ISA, as reported by Çevirim-Papaioannou et al. [18].

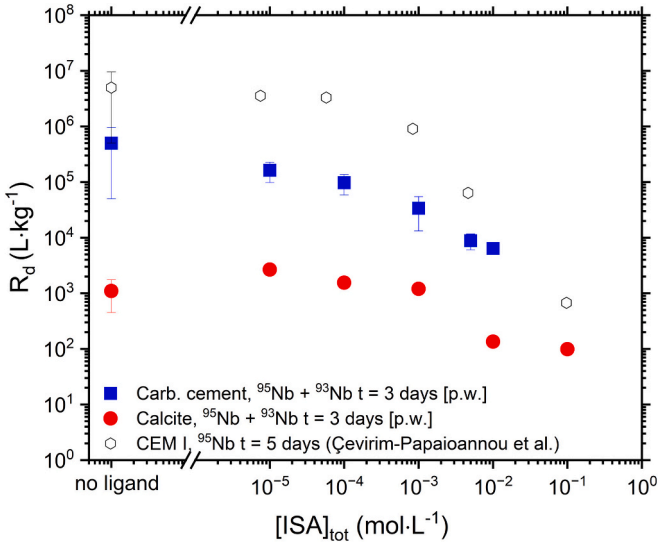

Fig. 7. Impact of ISA on the R_d values for the uptake of Nb(V) by calcite (this work), carbonated cement paste (this work) and cement paste CEM I (Çevirim-Papaioannou et al. [18]). All experiments conducted at S/L = 1 g·L^{-1} and $[Nb(V)]_{tot} = 1.0 \cdot 10^{-9}$ M, except otherwise indicated.

A relatively weak impact of ISA on the uptake of Nb(V) can be observed in Fig. 7 for both calcite and carbonated cement paste, with a negligible effect of ISA at ligand concentrations $\leq 1 \cdot 10^{-3}$ M. A decrease of ~1 log-units in R_d values is quantified at [ISA] = 0.1 M. In spite of the lacking thermodynamic data for this system, this observation is attributed primarily to the formation of Nb(V)-ISA complexes under the investigated boundary conditions. Note that a greater impact of ISA on Nb(V) sorption was reported for cement paste CEM I at pH ≈ 13.6 (white symbols in Fig. 7). The formation of more stable Nb(V)-ISA complexes is possibly expected in the hyperalkaline conditions defined by fresh cement, compared to the weakly alkaline conditions investigated in this work. As reported for other M-ISA systems (M = Ni(II), Zr(IV), Pu(IV)), the deprotonation of several alcohol groups of ISA under hyperalkaline pH conditions and the presence of a hard Lewis acid / metal ion expectedly results in the further stabilization of the M-ISA complexes in the aqueous phase [15,38,39]. Other parameters (*e.g.*, surface charge, concentration of Ca in the aqueous phase, sorption of ISA on the solid phase, *etc.*) can contribute as well to the differential behaviour observed for the uptake of Nb(V) at pH ≈ 8.3–8.5 (calcite, carbonated cement) and pH ≈ 13.6 (fresh cement).

According to thermodynamic calculations the formation of the complex $CaISA^+$ is expected to take place in the weakly alkaline conditions of this study. Fig. 8a shows the evolution of Ca concentration in equilibrium with calcite under increasing ISA concentration, whereas Fig. 8b displays the fraction diagram of Ca under the variation of ISA concentration, as calculated with the ThermoChimie database [22]. These calculations underpin the weak interaction between Ca^{2+} and ISA^- at pH ≈ 8.3, conditions under which all alcohol groups of ISA remain protonated. The speciation of ISA is dominated by the free ISA^- at this pH, even with increasing pH (see Fig. SI-3) and therefore only a minor dissolution of calcite takes place at $[ISA]_{tot} > 0.03$ M (estimated as 3.4 % at $[ISA]_{tot} = 0.04$ M, for systems with S/L = 1 g·L^{-1}), whereas the possible precipitation of $Ca(ISA)_2(cr)$ is predicted above this ISA concentration (see Fig. 8b). Thus, the minor fraction of calcite dissolved due to the formation of the $CaISA^+$ complex cannot be considered as responsible for the decrease in the uptake of Nb(V) observed at high ISA concentrations, as most of the solid phase remains available for sorption.

Fig. 9 shows the evolution of the R_d values for the uptake of Nb(V) by

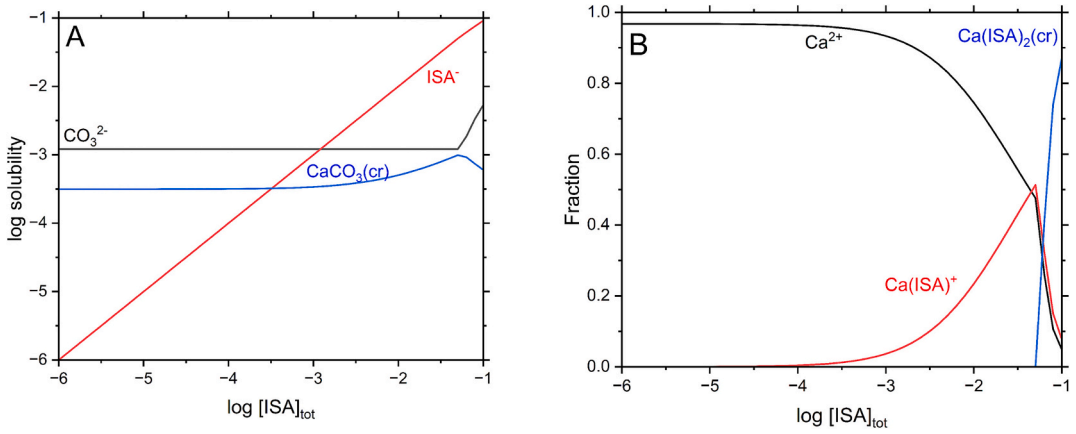

Fig. 8. (a) Impact of ISA on the solubility of $CaCO_3$(cr) at pH = 8.3 and $[C]_{tot} = 1.21 \cdot 10^{-3}$ M. (b) Ca aqueous speciation in presence of $[ISA]_{tot} = 10^{-6}$–10^{-1} M. Thermodynamic calculations were performed using the ThermoChimie database [22].

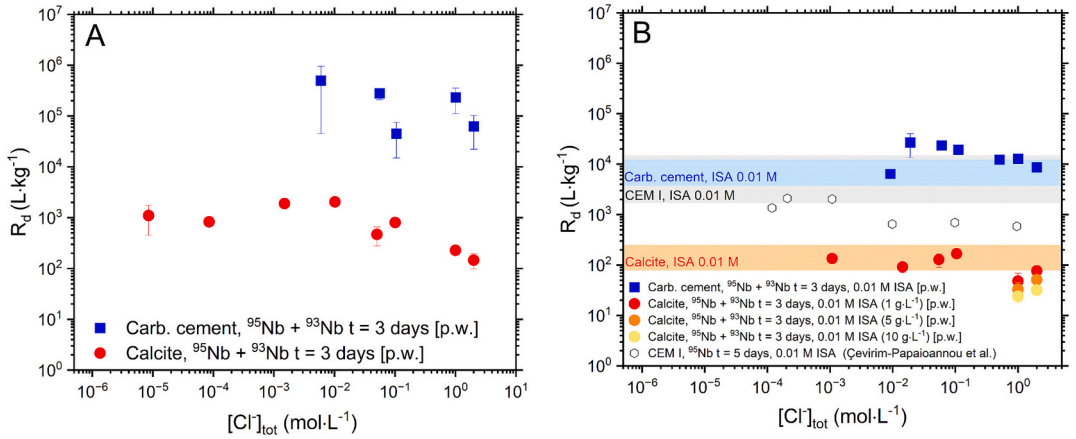

Fig. 9. Evolution of the R_d values (in $L \cdot kg^{-1}$) for the uptake of Nb(V) by calcite (this work), carbonated cement paste (this work) and cement paste CEM I (Çevirim-Papaioannou et al. [18]) at increasing chloride concentrations: (a) in the absence of ISA; (b) in the presence of $[ISA]_{tot} = 0.01$ M. All experiments conducted at S/L = 1 $g \cdot L^{-1}$ and $[Nb(V)]_{tot} = 1.0 \cdot 10^{-9}$ M, except otherwise indicated.

calcite and carbonated cement paste in the presence of increasing chloride concentrations, both in the absence (Fig. 9a) and in the presence (Fig. 9b) of $[ISA]_{tot} = 0.01$ M.

In the absence of ISA, chloride has a negligible impact on the uptake of Nb(V) by calcite at $[Cl^-]_{tot} \leq 0.1$ M, whereas a decrease of ~0.8 log-units in the R_d values is observed for $[Cl^-]_{tot} \geq 1$ M. At high chloride concentrations ($[Cl^-]_{tot} \geq 1$ M), a slight increase in the concentration of Ca was observed for the calcite system (see Fig. 10). This supports the partial dissolution of calcite, which can be quantified as 10–13 % of the initial calcite on the basis of a mass balance. However, this effect alone cannot justify the observed decrease in R_d. In carbonated cement systems, the presence of chloride has no evident impact on the sorption of Nb(V) up to $[Cl^-] = 2$ M. This observation possibly reflects a differential mechanism driving the uptake of Nb(V) in both systems, *e.g.*, involving amorphous silica in the carbonated cement paste, whose chemical behaviour might be less affected by high chloride concentrations.

Peiffert and co-workers investigated the solubility and hydrolysis of Nb(V) within $1 \leq pH \leq 9$ and $0.1\ mol \cdot kg^{-1} \leq [NaClO_4] \leq 6.0\ mol \cdot kg^{-1}$ [40]. At pH ≈ 9, the authors reported a drop in the Nb(V) concentration of *ca.* 1 order of magnitude between solubility data in 0.1 and 1.0 $mol \cdot kg^{-1}$ $NaClO_4$ (see Fig. 10 in [40] – modified version shown in the Supporting Information, see Fig. SI-4). This was interpreted as a decrease in the stability of the prevailing hydrolysis species at this pH, *i.e.*, $Nb(OH)_6^-$ and $Nb(OH)_7^{2-}$. Although such change in the speciation could affect sorption phenomena, we note that in the presence of Ca the

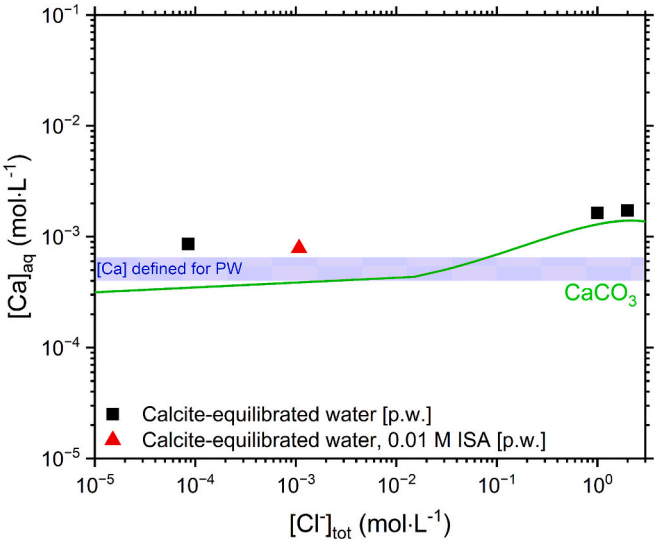

Fig. 10. Evolution of Ca concentration in calcite-equilibrated water with increasing $[Cl^-]_{tot}$, including Ca concentration at $[ISA]_{tot} = 0.01$ M. Thermodynamic calculations for $CaCO_3$(s) conducted using data selected in the ThermoChimie database [22].

formation of ternary aqueous complexes can be expected [33,41]. The lack of a complete thermodynamic model for the system under discussion hinders a more detailed mechanistic understanding of the processes driving the uptake of Nb(V) under these conditions.

Fig. 9b shows also the results of the sorption experiments with $[ISA]_{tot} = 0.01$ M and different chloride concentrations, ranging from $8.5{\cdot}10^{-5}$ M (calcite) and $5.0{\cdot}10^{-6}$ M (carbonated cement paste) (no additional chloride added, besides through pH correction) to 2 M. The results show that the R_d values are mostly consistent with the uptake of Nb(V) in the presence of ISA and absence of chloride. For the calcite system, similar results were obtained for different solid to liquid ratios (5 $g{\cdot}L^{-1}$ and 10 $g{\cdot}L^{-1}$). Only at the highest chloride concentration investigated ($[Cl^-] = 2$ M), a small decrease of ~0.2 log units in the R_d values of Nb(V) is observed for calcite and carbonated cement paste, although the decrease can be also considered within the uncertainties of the R_d measurements. The results obtained for the quaternary system support that chloride has a minor additive impact on the retention of Nb (V), while the uptake of Nb is primarily affected by ISA.

4. Summary and conclusions

The retention of niobium(V) by calcite and carbonated cement systems was comprehensively studied using a combination of ^{93}Nb (stable) and ^{95}Nb ($t_{1/2} = 35.0$ days). The investigated solid phases are taken as representative of the degradation stage IV of cement.

The commercial calcite used in the experiments was characterized by a high crystallinity and small BET surface area, *i.e.*, ≈ 0.7 $m^2{\cdot}g^{-1}$. Calcite was identified as main phase in the carbonated cement paste CEM I, although a significant fraction (26.4 wt%) of amorphous phase remains in the form of SiO_2 gel and C-S-H with low Ca/Si ratio. Carbonated cement paste was characterized by a significantly larger BET surface area, *i.e.*, ≈ 60 $m^2{\cdot}g^{-1}$. The concentration of natural niobium present in both solid materials was quantified as $[^{93}Nb] = 3.2{\cdot}10^{-5}$ $mol{\cdot}kg^{-1}$ (carbonated cement paste) and $[^{93}Nb] < 2.1{\cdot}10^{-9}$ $mol{\cdot}kg^{-1}$ (calcite, as detection limit of the technique).

Lower distribution ratios are quantified for the uptake of Nb(V) by calcite at short contact times ($t = 3$ days, $R_d \approx 10^3$ $L{\cdot}kg^{-1}$). A steady increase in the distribution ratios is observed with time, resulting in $R_d > 2{\cdot}10^4$ $L{\cdot}kg^{-1}$ at $t = 89$ days. These observations are tentatively explained as a fast adsorption of Nb(V) on the calcite surface, followed by a slow incorporation driven by calcite recrystallization. Manifestly stronger uptake of Nb(V) is determined for carbonated cement systems ($R_d \approx 8{\cdot}10^5$ $L{\cdot}kg^{-1}$). This differential behaviour is explained by the presence of SiO_2 gel and a small fraction of C-S-H phases with low Ca/Si ratio, which overall offer a much greater surface area than calcite. In addition, the presence of two different types of $CaCO_3$ in the carbonated sample proved by Raman spectroscopy may also affect the adsorption assuming that defective calcite shows much smaller crystal size and higher surface. Indeed, R_d values of calcite and carbonated cement paste level-off when normalized by surface area, thus highlighting the relevance of an adequate knowledge of the surface properties when comparing sorption behaviour of different materials.

Considering the presence of ^{93}Nb in the degraded cement paste, isotopic exchange needs to be taken into account as potential mechanism contributing to the retention of other niobium isotopes, *e.g.*, ^{95}Nb (this work) or ^{94}Nb (repository conditions). Further studies involving synchrotron-based techniques are planned to gain further insight on the mechanisms driving the uptake of niobium in calcite and degraded cement systems.

ISA has a minor to moderate impact on the uptake of Nb, both for calcite and carbonated cement systems. The decrease in R_d values observed at high ligand concentrations is attributed to the formation of Nb(V)–ISA complexes. However, the impact on sorption is weaker compared to observations reported for the degradation stage I of cement at pH ≈ 13.6. Such differences could be partly explained by the greater stability of the Nb(V)-ISA complexes under hyperalkaline conditions, although other parameters (*e.g.*, surface charge, concentration of Ca in the aqueous phase, sorption of ISA on the solid phase, *etc.*) can contribute as well to the differential behaviour. Dedicated thermodynamic studies may help to unravel this uncertainty. Chloride has a weak impact on sorption of Nb(V). The effect in R_d is more remarkable in calcite than in carbonated cement paste, which possibly reflects that a different mechanism is driving the uptake of Nb(V) in both systems.

This work provides the first quantitative description of the uptake of niobium by calcite and carbonated cement materials, which are representative of the degradation stage IV of cement. This information allows the correct quantification of the retention of niobium and a reliable assessment of its mobility in the context of the Safety Case for underground or near-surface repositories for nuclear waste.

CRediT authorship contribution statement

Nils Huber: Writing – review & editing, Writing – original draft, Methodology, Investigation, Formal analysis. **R.E. Guidone:** Writing – review & editing, Supervision, Methodology. **X. Gaona:** Writing – review & editing, Supervision, Project administration, Funding acquisition, Conceptualization. **K. Garbev:** Writing – review & editing, Methodology, Investigation, Formal analysis. **M. López-García:** Writing – review & editing, Methodology, Investigation. **L. Alcubierre:** Methodology, Investigation. **F. Bocchese:** Writing – review & editing, Project administration, Conceptualization. **S. Brassinnes:** Writing – review & editing, Project administration, Conceptualization. **M. Altmaier:** Writing – review & editing, Project administration, Funding acquisition, Conceptualization. **H. Geckeis:** Writing – review & editing, Supervision.

Declaration of competing interest

The authors declare the following financial interests/personal relationships which may be considered as potential competing interests: KIT-INE reports financial support was provided by ONDRAF-NIRAS. If there are other authors, they declare that they have no known competing financial interests or personal relationships that could have appeared to influence the work reported in this paper.

Acknowledgments

This work was partly funded by ONDRAF-NIRAS, Belgium (contract number CCHO 2015-0707/00/03). Markus Fuss, Annika Fried, Stephanie Kraft, Stefanie Kuschel and Tanja Kisely (all KIT-INE) are gratefully acknowledged for the analytical characterization of the investigated samples (gamma spectrometry, ICP–MS / OES, alkaline fusion, TOC / TIC / BET). We thank Thomas Sittel and Dieter Schild (KIT-INE) for the NMR characterization of ISA stock solutions and SEM-EDX imaging of the calcite.

Appendix A. Supplementary data

Supplementary data to this article can be found online at https://doi.org/10.1016/j.cemconres.2025.107952.

Data availability

All the data are included in supporting information.

References

[1] C.F. Baes, R.E. Mesmer, The hydrolysis of cations, Wiley, 1976.
[2] A.J. Bard, R. Parsons, J. Jordan, Standard potentials in aqueous solution, Marcel Dekker Inc., 1985.
[3] P.L. Brown, C. Ekberg, Hydrolysis of metal ions, Wiley, 2016.
[4] ONDRAF/NIRAS, Hoofdstuk 14 - Veiligheidsevaluatie - Langetermijnveiligheid - Veiligheidsrapport voor de oppervlaktebergingsinrichting van categorie A-afval te

Dessel. Category A (Technical Report NIROND-TR 2011-14 V3),. Brussels, Belgium, 2019.
[5] M. Ochs, D. Mallants, L. Wang, Radionuclide and metal sorption on cement and concrete, Springer, 2016.
[6] E. Wieland, in: Paul Scherrer Institute (PSI) (Ed.), Sorption data base for the cementitious near-field of L/ILW and ILW repositories for provisional safety analyses for SGT-E2, 2014.
[7] D. Jacques, Benchmarking of the Cement Model and detrimental chemical reactions including temperature dependent parameters, project near surface disposal of category A waste at Dessel, NIROND-TR, 2008.
[8] Z. Shi, B. Lothenbach, M.R. Geiker, J. Kaufmann, A. Leemann, S. Ferreiro, J. Skibsted, Experimental studies and thermodynamic modeling of the carbonation of Portland cement, metakaolin and limestone mortars, Cem. Concr. Res. 88 (2016) 60–72.
[9] B. Lothenbach, G. Le Saout, M.B. Haha, R. Figi, E. Wieland, Hydration of a low-alkali CEM III/B–SiO2 cement (LAC), Cem. Concr. Res. 42 (2012) 410–423.
[10] A. Schöler, B. Lothenbach, F. Winnefeld, M. Zajac, Hydration of quaternary Portland cement blends containing blast-furnace slag, siliceous fly ash and limestone powder, Cem. Concr. Compos. 55 (2015) 374–382.
[11] K. Vercammen, M. Glaus, L.R. Van Loon, Complexation of Th (IV) and Eu (III) by α-isosaccharinic acid under alkaline conditions, Radiochim. Acta 89 (2001) 393–402.
[12] J. Tits, E. Wieland, M. Bradbury, The effect of isosaccharinic acid and gluconic acid on the retention of Eu (III), am (III) and Th (IV) by calcite, Appl. Geochem. 20 (2005) 2082–2096.
[13] X. Gaona, V. Montoya, E. Colàs, M. Grivé, L. Duro, Review of the complexation of tetravalent actinides by ISA and gluconate under alkaline to hyperalkaline conditions, J. Contam. Hydrol. 102 (2008) 217–227.
[14] W. Hummel, F.J. Mompean, M. Illemassène, J. Perrone, Chemical thermodynamics of compounds and complexes of U, Np, Pu, Am, Tc, Se, Ni and Zr with selected organic ligands, Elsevier, Amsterdam, 2005.
[15] M.R. González-Siso, X. Gaona, L. Duro, M. Altmaier, J. Bruno, Thermodynamic model of Ni (II) solubility, hydrolysis and complex formation with ISA, Radiochim. Acta 106 (2018) 31–45.
[16] H. Hyvönen, M. Orama, H. Saarinen, R. Aksela, Studies on biodegradable chelating ligands: complexation of iminodisuccinic acid (ISA) with cu (II), Zn (II), Mn (II) and Fe (III) ions in aqueous solution, Green Chem. 5 (2003) 410–414.
[17] L. Wang, E. Martens, D. Jacques, P. De Canniere, D. Mallants, J. Berry, Review of sorption values for the cementitious near field of a near-surface radioactive waste disposal facility, 2012.
[18] N. Çevirim-Papaioannou, Y. Jo, K. Franke, M. Fuss, B. de Blochouse, M. Altmaier, X. Gaona, Uptake of niobium by cement systems relevant for nuclear waste disposal: impact of ISA and chloride, Cem. Concr. Res. 153 (2022) 106690.
[19] I. Pointeau, C. Landesman, N. Coreau, C. Moisan, P. Reiller, Am (III), Zr (IV), Pu (IV), Nb (V), U (VI) et Tc (IV) par les Matériaux Cimentaires Dégradés, CEA report, (2004) 03–037, 2004.
[20] Y. Jo, N. Çevirim-Papaioannou, K. Franke, M. Fuss, M. Pedersen, B. Lothenbach, B. de Blochouse, M. Altmaier, X. Gaona, Effect of ISA and chloride on the uptake of niobium (V) by hardened cement paste and CSH phases: quantitative description and mechanistic understanding, Cem. Concr. Res. 172 (2023) 107233.
[21] N. Huber, R.E. Guidone, X. Gaona, K. Garbev, S. Brassinnes, M. Altmaier, H. Geckeis, Impact of ISA and chloride on the uptake of Nb(V) by calcite and carbonated cement paste, in: 10th International Conference on Nuclear and Radiochemistry, 2024.
[22] B. Madé, W. Bower, S. Brassinnes, E. Colàs, L. Duro, P. Blanc, A. Lassin, L. Harvey, J. Begg, Recent developments in ThermoChimie–A thermodynamic database used in radioactive waste management, Appl. Geochem. 180 (2025) 106273.
[23] F. Heberling, L. Paulig, Z. Nie, D. Schild, N. Finck, Morphology controls on calcite recrystallization, Environ. Sci. Technol. 50 (2016) 11735–11741.
[24] J. Kalkreuth, A. Ullrich, K. Garbev, D. Merz, P. Stemmermann, D. Stapf, Accelerated carbonation of hardened cement paste: quantification of calcium carbonate via ATR infrared spectroscopy, J. Am. Ceram. Soc. 107 (2024) 2627–2640.
[25] N.V. Vagenas, A. Gatsouli, C.G. Kontoyannis, Quantitative analysis of synthetic calcium carbonate polymorphs using FT-IR spectroscopy, Talanta 59 (2003) 831–836.
[26] N. Cevirim-Papaioannou, Y. Jo, K. Franke, M. Fuss, B. de Blochouse, M. Altmaier, X. Gaona, Uptake of niobium by cement systems relevant for nuclear waste disposal: impact of ISA and chloride, Cem. Concr. Res. 153 (2022).
[27] F. Heberling, B. Brendebach, D. Bosbach, Neptunium (V) adsorption to calcite, J. Contam. Hydrol. 102 (2008) 246–252.
[28] X. Zhang, J. Guo, S. Wu, F. Chen, Y. Yang, Divalent heavy metals and uranyl cations incorporated in calcite change its dissolution process, Sci. Rep. 10 (2020) 16864.
[29] E. Elzinga, R. Reeder, X-ray absorption spectroscopy study of Cu2+ and Zn2+ adsorption complexes at the calcite surface: implications for site-specific metal incorporation preferences during calcite crystal growth, Geochim. Cosmochim. Acta 66 (2002) 3943–3954.
[30] T. Stumpf, M.M. Fernandes, C. Walther, K. Dardenne, T. Fanghänel, Structural characterization of am incorporated into calcite: a TRLFS and EXAFS study, J. Colloid Interface Sci. 302 (2006) 240–245.
[31] S. Hellebrandt, S. Hofmann, N. Jordan, A. Barkleit, M. Schmidt, Incorporation of Eu (III) into calcite under recrystallization conditions, Sci. Rep. 6 (2016) 33137.
[32] A.R. Chakhmouradian, E.P. Reguir, R.D. Kressall, J. Crozier, L.K. Pisiak, R. Sidhu, P. Yang, Carbonatite-hosted niobium deposit at Aley, northern British Columbia (Canada): mineralogy, geochemistry and petrogenesis, Ore Geol. Rev. 64 (2015) 642–666.
[33] Y. Jo, K. Garbev, N. Çevirim-Papaioannou, O.D. Blanco, B. de Blochouse, M. Altmaier, X. Gaona, Solubility of niobium (V) in cementitious systems relevant for nuclear waste disposal: characterization of the solubility-controlling solid phases, J. Hazard. Mater. 440 (2022) 129810.
[34] J. Tits, E. Wieland, C. Müller, C. Landesman, M. Bradbury, Strontium binding by calcium silicate hydrates, J. Colloid Interface Sci. 300 (2006) 78–87.
[35] S. Baker, R. McCrohon, P. Oliver, N. Pilkington, The sorption of niobium, tin, iodine and chlorine onto Nirex reference vault backfill, MRS Online Proceedings Library (OPL) 333 (1993) 719.
[36] I. Pointeau, C. Landesman, N. Coreau, N. Moisan, P. Reiller, Etude de la retention chimique des radionucleides Cs(I), Am(III), Zr(IV), Pu(IV), Nb(V), U(VI), Tc(IV) par les matériaux cimentaires degrades, CEA/DEN/SAC Report RT DPC/SECR 03-037, 2004.
[37] Y. Tachi, M. Mihara, T. Suyama, Data acquisition for radionuclide sorption on barrier materials for performance assessment of geological disposal of TRU wastes, Japan Atomic Energy Agency, JAEA-Data/Code 2019-021, 2020.
[38] A. Tasi, X. Gaona, D. Fellhauer, M. Böttle, J. Rothe, K. Dardenne, R. Polly, M. Grivé, E. Colàs, J. Bruno, Thermodynamic description of the plutonium–α-d-isosaccharinic acid system I: solubility, complexation and redox behavior, Appl. Geochem. 98 (2018) 247–264.
[39] T. Kobayashi, T. Teshima, T. Sasaki, A. Kitamura, Thermodynamic model for Zr solubility in the presence of gluconic acid and isosaccharinic acid, J. Nucl. Sci. Technol. 54 (2017) 233–241.
[40] C. Peiffert, C. Nguyen-Trung, D. Palmer, J.-P. Laval, E. Giffaut, Solubility of B-Nb 2 O 5 and the hydrolysis of niobium (V) in aqueous solution as a function of temperature and ionic strength, J. Solut. Chem. 39 (2010) 197–218.
[41] T. Yamaguchi, S. Ohira, K. Hemmi, L. Barr, A. Shimada, T. Maeda, Y. Iida, Consideration on modeling of Nb sorption onto clay minerals, Radiochim. Acta 108 (2020) 873–877.